High-Cooperativity Coupling of a Rare-Earth Spin Ensemble to a Superconducting Resonator Using Yttrium Orthosilicate as a Substrate

Gavin Dold,[1,2,*] Christoph W. Zollitsch,[1] James O'Sullivan,[1] Sacha Welinski,[3] Alban Ferrier,[3,4] Philippe Goldner,[3] S.E. de Graaf,[2] Tobias Lindström,[2] and John J.L. Morton[1,5,†]

[1] *London Centre for Nanotechnology, University College London, London WC1H 0AH, United Kingdom*
[2] *National Physical Laboratory, Hampton Road, Teddington TW11 0LW, United Kingdom*
[3] *Université PSL, Chimie ParisTech, CNRS, Institut de Recherche de Chimie Paris, 75005 Paris, France*
[4] *Faculté des Sciences et Ingénierie, Sorbonne Université, 75005 Paris, France*
[5] *Department of Electronic and Electrical Engineering, UCL, London WC1E 7JE, United Kingdom*

Yttrium orthosilicate (Y_2SiO_5, or YSO) has proved to be a convenient host for rare-earth ions used in demonstrations of microwave quantum memories and optical memories with microwave interfaces and shows promise for coherent microwave-optical conversion owing to its favorable optical and spin properties. The strong coupling required by such microwave applications could be achieved using superconducting resonators patterned directly on Y_2SiO_5 and hence we investigate here the use of Y_2SiO_5 as an alternative to sapphire or silicon substrates for superconducting-hybrid-device fabrication. A NbN resonator with frequency 6.008 GHz and low-power quality factor $Q \approx 400\,000$ is fabricated on a Y_2SiO_5 substrate doped with isotopically enriched ^{145}Nd. Measurements of dielectric loss yield a loss tangent $\tan\delta = 4 \times 10^{-6}$, comparable to that of sapphire. Electron spin resonance (ESR) measurements performed using the resonator show the characteristic angular dependence expected from the anisotropic ^{145}Nd spin and the coupling strength between the resonator and the electron spins is in the high-cooperativity regime ($C = 30$). These results demonstrate that Y_2SiO_5 is an excellent substrate for low-loss, high-Q microwave resonators, especially in applications for coupling to optically accessible rare-earth spins.

I. INTRODUCTION

Rare-earth ions (REIs) in crystals are promising candidate systems for quantum-information applications, as they possess electron and nuclear spins as well as optical transitions at telecom wavelengths. Coherence times in these systems range from milliseconds [1] for microwave excitations stored in an electron spin to hours [2,3] for optically accessible nuclear excitations. REIs typically possess large g factors (beneficial for strong coupling), have a variety of nuclear spin states, and offer opportunities for optical pumping. Such properties have led to proposals for using rare-earth ions as a multimode microwave quantum memory [4], a photonic memory for a quantum repeater [5], and as a microwave-optical transducer [6,7] for use in quantum networks [8].

Yttrium orthosilicate (Y_2SiO_5) is a widely used crystalline host for REIs in such quantum-information applications, as its constituent elements provide an environment with a low background of nuclear magnetic moments that would otherwise contribute to spin decoherence and inhomogeneous broadening. The narrow homogeneous linewidths—for example, down to 3.5 kHz for the 883 nm transition [9] in $Nd^{3+} : Y_2SiO_5$—have been exploited as an optical quantum memory [10,11] enabling storage of entangled states [12] and teleportation with 93% fidelity [13].

While optical-storage experiments using REIs in Y_2SiO_5 can make use of a suitably optically dense medium, for microwave storage a cavity is employed to achieve a coupling between an ensemble of REIs and the microwave-cavity field, so that excitations can be coherently exchanged between the two. This can be achieved with three-dimensional (3D) microwave cavities [7], which offer homogeneous B_1 fields and spatial mode matching between microwave and optical fields, or planar superconducting resonators with small mode volumes and quality factors over 10^5, to yield high spin-number sensitivities [14] and act as an interface between superconducting qubits and spin ensembles [15]. Dielectric resonators fabricated from rare-earth-doped crystals such as YAG ($Y_3Al_5O_{12}$) [16] have used resonant modes with $Q \approx 10^4$ to drive ESR transitions with cooperativity $C \approx 600$, while

_____

*gavin.dold.15@ucl.ac.uk
†jjl.morton@ucl.ac.uk

planar superconducting resonators have been coupled to rare earths ($Q \approx 10^3$, $C = 36$, [17]), group V donors in silicon [14,18], nitrogen-vacancy (NV) centers in diamond [15], and ruby ($Al_2O_3 : Cr^{3+}$) [19].

Experiments coupling superconducting resonators to doped crystals have typically used a *flip-chip* approach, with the sample glued or mechanically pressed onto the resonator chip [17]. This has the drawback of complicating the fabrication process and creates an additional interface layer between the resonator and sample, increasing dielectric losses from spurious two-level systems (TLSs) in the interface [20], as well as a variable gap between the device and the spins, which is less controllable than fabrication on the substrate itself.

Common substrates for superconducting resonators include silicon and sapphire (Al_2O_3) [21]. Dielectric losses in these are usually quantified by the loss tangent $\tan\delta$, which describes the ratio between the imaginary and real components of the complex permittivity of the material. This creates a limit on the quality factor achievable in superconducting resonators: $Q = 1/\tan\delta$. For high-Q devices, sapphire is often preferred due to its low loss tangent [22] $\tan\delta < 10^{-5}$, leading to quality factors approaching 10^6.

In this work, we investigate the suitability of using Y_2SiO_5 itself as a substrate for fabrication of planar superconducting devices. We fabricate a resonator on the polished surface of a Nd-doped Y_2SiO_5 sample and find that the device has a Q factor $> 10^5$ at low powers due to its low loss tangent $\tan\delta = 4 \times 10^{-6}$. We observe an anisotropic ESR spectrum matching that from simulations and measure the coupling strength between the resonator and the electron spin to be in the high-cooperativity regime. These results suggest that fabrication on doped Y_2SiO_5 is compatible with high-Q devices while simultaneously enabling a coupling to crystals doped with rare-earth ions and could be a promising route toward scalable hybrid superconductor-spin quantum circuits.

II. THE DEVICE

The device is a lumped-element superconducting resonator, fabricated on a Czochralski-grown single crystal of Y_2SiO_5 [23] doped with 10 ppm isotopically purified ^{145}Nd. The crystal is cut into a 5 mm × 5 mm × 460 μm chip along the principal dielectric axes (D_1, D_2, and b) and a face perpendicular to b is polished for thin-film growth. Y_2SiO_5 has two inequivalent crystal sites where a Y^{3+} ion can be substituted by a rare-earth RE^{3+} ion. The large ionic radius of Nd^{3+} results in the larger crystal Site 1 being preferentially populated [1], resulting in a stronger signal from site 1 over site 2. Due to the crystal's C_{2h}^6 ($C2/c$) space group, each site has two orientations related by a π rotation around the crystal b axis. These two orientations are termed *subsites* and their ESR properties are degenerate
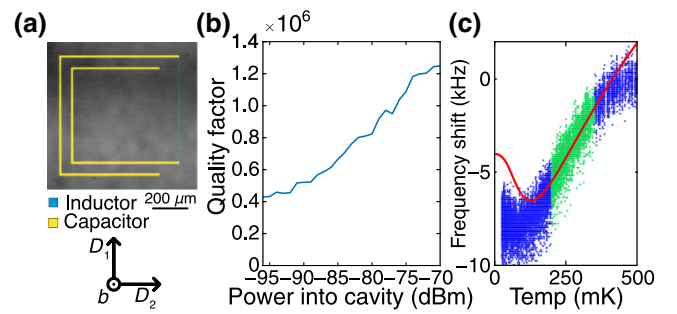

FIG. 1. (a) A false-color micrograph of the superconducting thin-ring resonator on $^{145}Nd : Y_2SiO_5$ substrate. (b) The power dependence of the loaded quality factor at zero field. At high powers, the TLSs begin to saturate, resulting in an increase in Q [24]. (c) The frequency shift of the resonator as a function of the temperature, from which a fit to theory [22] (red) of the gradient of the linear section (green) yields the loss tangent $\tan\delta = 4 \times 10^{-6}$.

for B_0 fields applied in the D_1-D_2 plane or parallel to the b axis.

The resonator consists of a 2 μm wire, which functions as an inductor due to the constriction increasing the contribution of kinetic inductance, and a pair of 10-μm-thick capacitive arms separated by a 50-μm gap. The use of narrow features increases the resilience of the resonator to the applied magnetic field and the large gap between the capacitive arms reduces the peak electric field of the resonator, decreasing its susceptibility to dielectric losses from two-level systems. This forms a lumped-element resonator, seen in the micrograph in Fig. 1, which generates an oscillating B_1 magnetic field around the inductor that can drive ESR transitions. Details of this resonator design's properties in an applied magnetic field will be described in a future publication.

Fabrication consists of 40 nm of sputtered NbN being patterned by photolithography and a SF_6/Ar reactive-ion-etch process. The patterned chip is enclosed within a 3D copper cavity ($Q \approx 100$) to suppress spontaneous emission from the resonator to the environment [14]. This is installed in the bore of a vector magnet in a dilution refrigerator at 10 mK (measured at the mixing chamber plate) and probed using a vector network analyser (VNA) at zero applied magnetic field.

The lumped-element resonator has a frequency of 6.008 GHz and an asymmetric lineshape due to interference with the background transmission of the 3D cavity. Fitting with a Fano resonance [25] yields a quality factor $Q \approx 400\,000$ in the low-power limit in Fig. 1. By tracking the center frequency versus the temperature [24], we find that the dielectric losses in the device are comparable to those of resonators fabricated on sapphire [22,26], with a loss tangent $\tan\delta = 4 \times 10^{-6}$, where the filling factor $F \approx \frac{1}{2}$ representing the fraction of the magnetic field penetrating the substrate has been factored out.

This demonstrates that Y_2SiO_5 is well suited for devices incorporating resonators and superconducting qubits, which are typically susceptible to dielectric losses from TLSs [27], while also incorporating doped spins for cavity quantum electrodynamics (QED).

III. ELECTRON SPIN RESONANCE

A. ESR spectrum

Having studied the resonator, we now use it to perform ESR to characterize the Nd spins in the Y_2SiO_5 that are coupled to the resonator. A magnetic field B_0 is applied in the plane of the superconducting thin film, roughly perpendicular to the Y_2SiO_5 crystal b axis, to minimize the magnetic flux threaded through the superconductor. The field is swept up to 360 mT and the resonator is used to observe ESR transitions, monitoring changes to its center frequency tracked with a VNA. By this method, a series of spectra are taken as a function of the B_0 orientation in the D_1-D_2 plane to extract the angular dependence, or "roadmap", of ESR line positions, in order to confirm the presence of Nd spins in the substrate and measure their coupling to the resonator.

For an electron spin **S** coupled to a nuclear spin **I**, the Hamiltonian accounting for the electron Zeeman and hyperfine terms is $H = \mu_B \mathbf{B}^T \mathsf{g} \hat{\mathbf{S}} + \hat{\mathbf{S}}^T \mathsf{A} \hat{\mathbf{I}}$. The anisotropy of Y_2SiO_5 results in the parameters g and A being tensors, previously calculated from spectroscopic studies of Site 1

of ^{145}Nd : Y_2SiO_5 at 9.4 GHz [28] as follows:

$$\mathsf{g} = \begin{pmatrix} 1.30 & 0.62 & 0.22 \\ 0.62 & -2.07 & 1.62 \\ 0.22 & 1.62 & -2.86 \end{pmatrix}_{(D_1,D_2,b)},$$

$$\mathsf{A} = \begin{pmatrix} -37.1 & -99.9 & -83.4 \\ -99.9 & -589.2 & 169.4 \\ -83.4 & 169.4 & -678.4 \end{pmatrix}_{(D_1,D_2,b)} \text{MHz.}$$

A characteristic ESR spectrum (B_0 along the D_1 axis) is plotted in Fig. 2(b). We observe a series of eight ESR transitions indicated in Fig. 2(a), corresponding to the ^{145}Nd nuclear spin $\left(I = \frac{7}{2}\right)$ in Site 1. A small misalignment between the D_1-D_2 and the superconductor planes breaks the degeneracy between the crystal subsites and causes a further splitting of each line into two.

The roadmap of the ESR spectrum with respect to the B_0-field angle is plotted in Fig. 2(c), with transitions marked by circles. The angular dependence seen in these spectra matches simulations well for Nd spins in Site 1 (blue), while we also observe a signal at lower magnetic fields (higher g factor), which we attribute to Site 2 (red). The full spin Hamiltonian of ^{145}Nd in Site 2, including hyperfine terms, has not been reported; therefore our simulations only account for the Zeeman term (i.e., the g tensor). Additional unidentified impurities are evident from the different angular dependencies of 2–3 transitions marked in green and black.
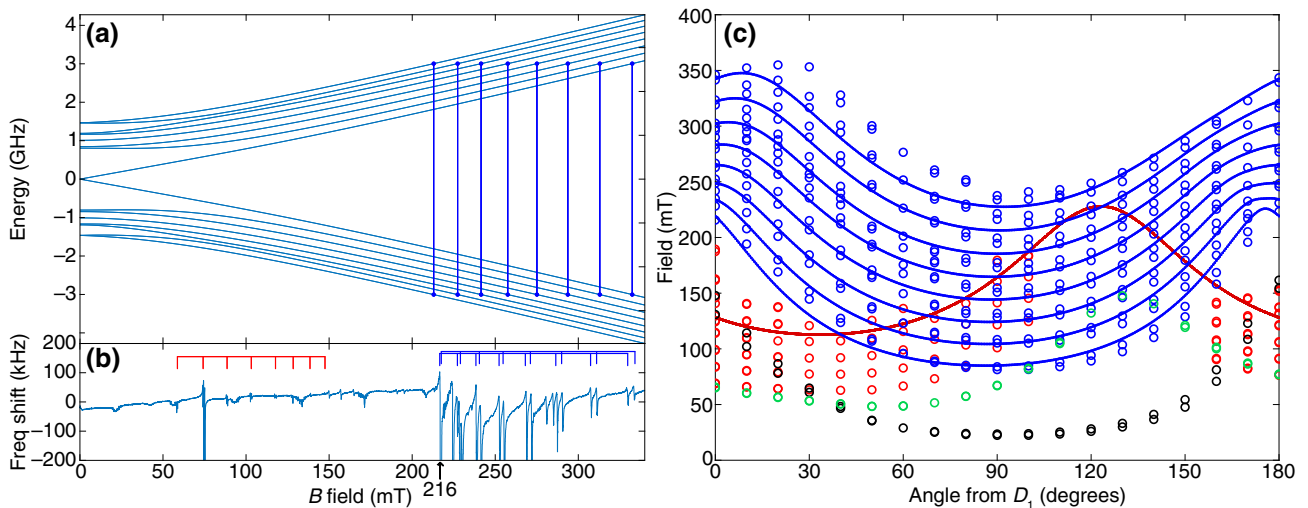

FIG. 2. (a) A Breit-Rabi diagram of ^{145}Nd in Y_2SiO_5 for magnetic field B_0 oriented along D_1, with ESR transitions at 6.008 GHz indicated. (b) The ESR spectrum with the magnetic field B_0 oriented along D_1, as measured with a VNA tracking the resonator center frequency. The quadratic dependence of the resonator frequency with the applied magnetic field has been subtracted. Transitions from Site 1 are indicated in blue and those from Site 2 in red. Two sets of Site-1 transitions are seen due to a broken subsite degeneracy. The avoided crossing studied in Sec. III B is indicated at $B_0 = 216$ mT. (c) The roadmap of ESR transition fields with respect to the B_0 angle from the D_1 axis, in the D_1-D_2 plane. The circles mark the positions of transitions from traces such as in (b), with Site 1 in blue and Site 2 in red. Signals from Site 2 between $110°$ and $150°$ could not be resolved due to weak transition amplitudes at these angles. The lines represent simulated data assuming an ideal rotation about the crystal b axis. For Site 2, we only show one line, as only the g tensor is known for this site. The green and black colors represent as-yet-unidentified impurities.

These measurements enable ESR transitions to be positively identified by comparing their angular dependence to simulations [29] and bulk ESR data, ensuring that further analysis of spin-resonator coupling properties can be clearly linked to a particular spin species.

B. High-cooperativity coupling

The highest-intensity ESR transition for ^{145}Nd in Site 1 with $m_I = \frac{7}{2}$ at $B_0 = 216$ mT along D_1 is selected for an evaluation of the spin-resonator coupling strength. Measuring the resonator S_{21} with a VNA while sweeping the magnetic field strength B, we observe the onset of an avoided crossing shown in Fig. 3. Fitting of the resonator frequency ω and linewidth κ at each field point [30] allows us to extract the coupling strength g_{ens}, the inhomogeneous spin-ensemble half-width γ_s, and the resonator half-width κ_c with

$$\omega = \omega_c - g_{ens}^2 \Delta/(\Delta^2 + \gamma_s^2),$$
$$\kappa = \kappa_c - g_{ens}^2 \gamma_s/(\Delta^2 + \gamma_s^2),$$

where $\Delta = m_0(B - B_0)/\hbar$ is the field detuning calculated from the spin magnetic moment $m_0 = \hbar(d\omega/dB_0)$. This accounts for cases where $d\omega/dB$ varies with B, as is the case for mixed-spin systems in the low-field limit or near zero first-order Zeeman (ZEFOZ) points.

From this, we extract $g_{ens} = 1.5$ MHz, $\gamma_s = 5.7$ MHz, and $\kappa_c = 13.2$ kHz. This corresponds to a high cooperativity $C = g_{ens}^2/\kappa_c\gamma_s = 30$.

For a bulk-doped sample, there is no clear single-spin coupling rate, as the $1/r$ decay of the field strength from the wire results in a B_1 inhomogeneity spanning orders of magnitude, while all spins in the sample contribute to the signal. However, a characteristic rate representing the average coupling strength over the spins contributing 50% of the measured signal can be calculated. This corresponds to a region within 4 μm of the wire with $N \approx 6 \times 10^8$ resonant ^{145}Nd spins in the same subsite, accounting for the thermal population in the $m_I = \frac{7}{2}$ ESR transition at 10 mK. From this, we derive a characteristic single-spin coupling rate $g_0 = g_{ens}/\sqrt{N} \approx 50$ Hz, leading to an expected Purcell enhanced emission rate [31] of $\Gamma_P = 4g_0^2/\kappa_c \approx 1$ Hz.

These results indicate that the coupling regime is limited by the spin line width $\gamma_s > g_{ens}$ or, equivalently, that the Nd spin ensemble is decohering at a faster rate than excitations are being exchanged between it and the resonator. Steps toward improving this coupling strength could include using a more strongly doped rare-earth sample to increase g_{ens}, although this could also increase γ_s, or exploiting the coherence-enhancing ZEFOZ transitions in REIs [32] to decrease γ_s. The significant B_1 inhomogeneity in this resonator design also poses challenges for performing coherent operations on the entire spin ensemble with pulsed ESR. This could be mitigated by coupling to implanted layers of REIs [29,33] or by using resonators designed to generate a more homogeneous B_1 field.
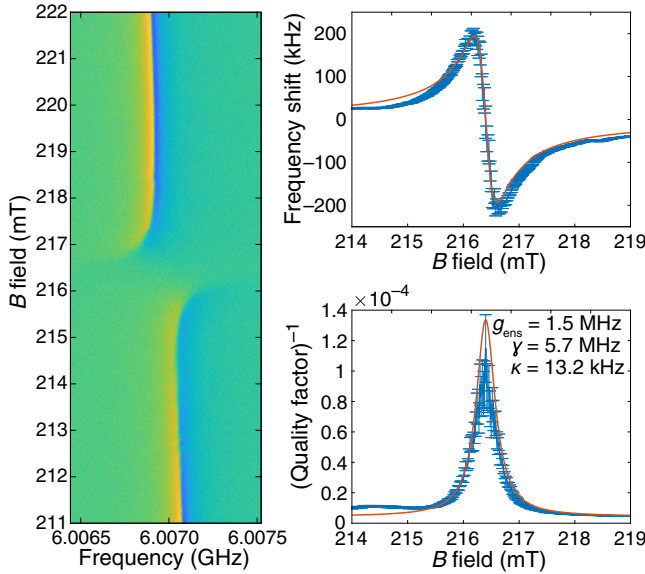

FIG. 3. Left: the onset of an avoided crossing when sweeping the B field through resonance. Right: the resonator frequency shift and quality factor as a function of the B-field strength when sweeping through resonance. The uncertainty in the resonator quality factor increases at the center of the transition due to a reduction in prominence of the resonance. A simultaneous fit to all resonances as a function of the magnetic field, using the equations in the main text, yields a dependence of the frequency and the quality factor with the field shown in red and a high-cooperativity coupling $C = 30$.

IV. CONCLUSION

We investigate the use of Y_2SiO_5 as an alternative to sapphire or silicon substrates for the fabrication of superconducting devices. The fabricated NbN lumped-element resonator has a quality factor $Q \approx 400\,000$ and a loss tangent $\tan\delta = 4 \times 10^{-6}$ comparable to that of sapphire [22] and yields a high-cooperativity coupling $C = 30$ between the resonator and a ^{145}Nd spin ensemble. These results demonstrate that Y_2SiO_5 is well suited for superconducting devices, while also enabling an interaction with optically accessible rare-earth spins.

Further studies of this device include performing pulsed ESR measurements in the high-cooperativity regime and measuring the coherence properties of the spin ensemble. The methods shown here are also applicable to other REIs in Y_2SiO_5; for example, Er, with its 1540-nm telecom-band optical transition [7], and Yb, which exhibits a large oscillator strength [34] and coherence-enhancing ZEFOZ

and near-ZEFOZ transitions [32]. It may also prove interesting to study the suitability as a substrate of other crystalline hosts for REIs, such as yttrium aluminium garnet (YAG), yttrium lithium fluoride (YLF), yttrium orthovanadate (YVO$_4$), and calcium tungstate (CaWO$_4$).

The fabrication of superconducting devices on crystals doped with REIs as demonstrated here shows promise for integrating these optical elements alongside the fast information processing available from superconducting qubits. This is an important step toward making a microwave-optical transducer capable of connecting such quantum processors within a quantum network. By exploiting the long coherence times available from REIs, this is also a route to integrating fast quantum electronics with a spin ensemble acting as a quantum memory.

ACKNOWLEDGMENTS

[1] G. Wolfowicz, H. Maier-Flaig, R. Marino, A. Ferrier, H. Vezin, J. J. L. Morton, and P. Goldner, Coherent Storage of Microwave Excitations in Rare-Earth Nuclear Spins, Phys. Rev. Lett. **114**, 170503 (2015).

[2] M. Zhong, M. P. Hedges, R. L. Ahlefeldt, J. G. Bartholomew, S. E. Beavan, S. M. Wittig, J. J. Longdell, and M. J. Sellars, Optically addressable nuclear spins in a solid with a six-hour coherence time, Nature **517**, 177 (2015).

[3] M. Rančić, M. P. Hedges, R. L. Ahlefeldt, and M. J. Sellars, Coherence time of over a second in a telecom-compatible quantum memory storage material, Nat. Phys. **14**, 50 (2017).

[4] S. Probst, H. Rotzinger, A. V. Ustinov, and P. A. Bushev, Microwave multimode memory with an erbium spin ensemble, Phys. Rev. B **92**, 014421 (2015).

[5] N. Sangouard, C. Simon, H. de Riedmatten, and N. Gisin, Quantum repeaters based on atomic ensembles and linear optics, Rev. Mod. Phys. **83**, 33 (2011).

[6] L. A. Williamson, Y. H. Chen, and J. J. Longdell, Magneto-Optic Modulator with Unit Quantum Efficiency, Phys. Rev. Lett. **113**, 1 (2014).

[7] X. Fernandez-Gonzalvo, Y. H. Chen, C. Yin, S. Rogge, and J. J. Longdell, Coherent frequency up-conversion of microwaves to the optical telecommunications band in an Er:YSO crystal, Phys. Rev. A—Atomic Mol. Opt. Phys. **92**, 1 (2015).

[8] H. J. Kimble, The quantum internet, Nature **453**, 1023 (2008).

[9] I. Usmani, M. Afzelius, H. de Riedmatten, and N. Gisin, Mapping multiple photonic qubits into and out of one solid-state atomic ensemble, Nat. Commun. **1**, 1 (2010).

[10] M. P. Hedges, J. J. Longdell, Y. Li, and M. J. Sellars, Efficient quantum memory for light, Nature **465**, 1052 (2010).

[11] P. Jobez, C. Laplane, N. Timoney, N. Gisin, A. Ferrier, P. Goldner, and M. Afzelius, Coherent Spin Control at the Quantum Level in an Ensemble-Based Optical Memory, Phys. Rev. Lett. **114**, 230502 (2015).

[12] C. Clausen, I. Usmani, F. Bussières, N. Sangouard, M. Afzelius, H. de Riedmatten, and N. Gisin, Quantum storage of photonic entanglement in a crystal, Nature **469**, 508 (2011).

[13] F. Bussieres, C. Clausen, A. Tiranov, B. Korzh, V. B. Verma, S. W. Nam, F. Marsili, A. Ferrier, P. Goldner, H. Herrmann, C. Silberhorn, W. Sohler, M. Afzelius, and N. Gisin, Quantum teleportation from a telecom-wavelength photon to a solid-state quantum memory, Nat. Photonics **8**, 775 (2014).

[14] A. Bienfait, J. J. Pla, Y. Kubo, M. Stern, X. Zhou, C. C. Lo, C. D. Weis, T. Schenkel, M. L. W. Thewalt, D. Vion, D. Esteve, B. Julsgaard, K. Moelmer, J. J. L. Morton, and P. Bertet, Reaching the quantum limit of sensitivity in electron spin resonance, Nat. Nanotechnol. **11**, 10 (2015).

[15] Y. Kubo, C. Grezes, A. Dewes, T. Umeda, J. Isoya, H. Sumiya, N. Morishita, H. Abe, S. Onoda, T. Ohshima, V. Jacques, A. Dréau, J. F. Roch, I. Diniz, A. Auffeves, D. Vion, D. Esteve, and P. Bertet, Hybrid Quantum Circuit with a Superconducting Qubit Coupled to a Spin Ensemble, Phys. Rev. Lett. **107**, 220501 (2011).

[16] W. G. Farr, M. Goryachev, J.-M. le Floch, P. Bushev, and M. E. Tobar, Evidence of dilute ferromagnetism in rare-earth doped yttrium aluminium garnet, Appl. Phys. Lett. **107**, 122401 (2015).

[17] S. Probst, H. Rotzinger, S. Wünsch, P. Jung, M. Jerger, M. Siegel, A. V. Ustinov, and P. A. Bushev, Anisotropic Rare-Earth Spin Ensemble Strongly Coupled to a Superconducting Resonator, Phys. Rev. Lett. **110**, 1 (2013).

[18] C. W. Zollitsch, K. Mueller, D. P. Franke, S. T. B. Goennenwein, M. S. Brandt, R. Gross, and H. Huebl, High cooperativity coupling between a phosphorus donor spin ensemble and a superconducting microwave resonator, Appl. Phys. Lett. **107**, 142105 (2015).

[19] D. I. Schuster, A. P. Sears, E. Ginossar, L. Dicarlo, L. Frunzio, J. J. L. Morton, H. Wu, G. A. D. Briggs, B. B. Buckley, D. D. Awschalom, and R. J. Schoelkopf, High-Cooperativity Coupling of Electron-Spin Ensembles to Superconducting Cavities, Phys. Rev. Lett. **105**, 140501 (2010).

[20] J. Burnett, L. Faoro, I. Wisby, V. L. Gurtovoi, A. V. Chernykh, G. M. Mikhailov, V. A. Tulin, R. Shaikhaidarov, V. Antonov, P. J. Meeson, A. Y. Tzalenchuk, and T. Lindström, Evidence for interacting two-level systems from the $1/f$ noise of a superconducting resonator, Nat. Commun. **5**, 4119 (2014).

[21] W. D. Oliver and P. B. Welander, Materials in superconducting quantum bits, MRS Bull. **38**, 816 (2013).

[22] T. Lindström, J. E. Healey, M. S. Colclough, C. M. Muirhead, and A. Y. Tzalenchuk, Properties of superconducting planar resonators at millikelvin temperatures, Phys. Rev. B—Condens. Matter Mater. Phys. **80**, 2 (2009).

[23] Z. Shoudu, W. Siting, S. Xingda, W. Haobing, Z. Heyu, Z. Shunxing, and X. Jun, Czochralski growth of rare-earth orthosilicates Y_2SiO_5 single crystals, J. Cryst. Growth **197**, 901 (1999).

[24] J. Zmuidzinas, Superconducting microresonators: Physics and applications, Ann. Rev. Condens. Matter Phys. **3**, 169 (2012).

[25] A. Bärnthaler, S. Rotter, F. Libisch, J. Burgdörfer, S. Gehler, U. Kuhl, and H. J. Stöckmann, Probing Decoherence Through Fano Resonances, Phys. Rev. Lett. **105**, 1 (2010).

[26] D. P. Pappas, M. R. Vissers, D. S. Wisbey, J. S. Kline, and J. Gao, Two level system loss in superconducting microwave resonators, IEEE Trans. Appl. Supercond. **21**, 871 (2011).

[27] L. Faoro and L. B. Ioffe, Quantum Two Level Systems and Kondo-Like Traps as Possible Sources of Decoherence in Superconducting Qubits, Phys. Rev. Lett. **96**, 1 (2006).

[28] H. Maier-Flaig, Master's thesis, Karlsrhue Institute of Technology, 2013.

[29] I. S. Wisby, S. E. de Graaf, R. Gwilliam, A. Adamyan, S. E. Kubatkin, P. J. Meeson, A. Y. Tzalenchuk, and T. Lindström, Angle-Dependent Microresonator ESR Characterization of Locally Doped Gd3+ : Al_2O_3, Phys. Rev. Appl. **6**, 024021 (2016).

[30] E. Abe, H. Wu, A. Ardavan, and J. J. L. Morton, Electron spin ensemble strongly coupled to a three-dimensional microwave cavity, Appl. Phys. Lett. **98**, 3 (2011).

[31] A. Bienfait, J. J. Pla, Y. Kubo, X. Zhou, M. Stern, C. C. Lo, C. D. Weis, T. Schenkel, D. Vion, D. Esteve, J. J. L. Morton, and P. Bertet, Controlling spin relaxation with a cavity, Nature **531**, 74 (2016).

[32] A. Ortu, A. Tiranov, S. Welinski, F. Fröwis, N. Gisin, A. Ferrier, P. Goldner, and M. Afzelius, Simultaneous coherence enhancement of optical and microwave transitions in solid-state electronic spins, Nat. Mater. **17**, 671 (2018).

[33] N. Kukharchyk, J. Pal, J. Rödiger, A. Ludwig, S. Probst, A. V. Ustinov, P. Bushev, and A. D. Wieck, Photoluminescence of focused ion beam implanted Er3+ : Y_2SiO_5 crystals, Phys. Status Solidi (RRL)—Rapid Res. Lett. **8**, 880 (2014).

[34] S. Welinski, A. Ferrier, M. Afzelius, and P. Goldner, High-resolution optical spectroscopy and magnetic properties of Yb^{3+} in Y_2SiO_5, Phys. Rev. B **94**, 155116 (2016).